Cerebellar modulation of gamma coherence between prefrontal cortex and hippocampus during spatial working memory decision making

Liu Y[1], McAfee SS[2], Sillitoe RV[3,4,5,6], Heck DH[1]

[1]Department of Anatomy and Neurobiology, University of Tennessee HSC, Memphis, TN 38163, USA

[2]Department of Diagnostic Imaging, St Jude Children's Research Hospital, Memphis, TN, 38112, US

[3]Department of Pathology and Immunology, Baylor College of Medicine

[4]Department of Neuroscience, Baylor College of Medicine

[5]Development, Disease Models & Therapeutics Graduate Program, Baylor College of Medicine

[6]Jan and Dan Duncan Neurological Research Institute of Texas Children's Hospital, 1250 Moursund Street, Suite 1325, Houston, Texas 77030, USA

Corresponding author:

Detlef Heck, Ph.D.

University of Tennessee Health Science Center

Dept. Anatomy & Neurobiology

855 Monroe Ave.

Memphis, TN 38163

Phone: +1 901 448 1678

E-mail: dheck@uthsc.edu

Abstract

Spatial working memory (SWM) in rodents jointly requires the medial prefrontal cortex (mPFC) and dorsal hippocampal CA1 region (dCA1). We show that the decision-making process in a SWM task is associated with increased coherence of gamma oscillations between the mPFC and dCA1, with the magnitude of coherence change correlated with decision outcome. Purkinje cells in the cerebellar lobulus simplex (LS) have been shown to represent mPFC and dCA1 gamma oscillation phase and phase differences. Here we show that the LS is causally involved in the modulation of decision-related mPFC-dCA1 gamma coherence and SWM performance. Previous studies reported a cerebellar involvement in modulating coherence between sensory and motor cortical areas. Together these findings suggest cerebellar modulation of cerebral cortical coherence as a possible universal mechanism of cerebrocerebellar interaction.

Summary

The cerebellum is involved in numerous cognitive functions, including working memory. Evidence for a cerebellar involvement in working memory comes from functional imaging studies of verbal or visual working memory in humans, showing localized activation of right cerebellar lobulus simplex (LS) and Crus I [1]. Animal studies have shown that normal place cell function in the hippocampus as well as spatial orientation behavior requires an intact cerebellum [2-6]. Neural tracing studies in mice revealed connections between the posterior cerebellar hemisphere and the hippocampus [5]. It is generally accepted that connections between the cerebellum and cerebral cortex are an anatomical requirement of cerebellar cognitive function. However, the nature of the neuronal interactions between the cerebral and cerebellar cortices as it relates to cognitive functions remains unclear. Addressing this question requires simultaneous observations of neuronal activity in communicating cerebral and cerebellar areas during the performance of a cognitive behavior involving these areas. The known involvement of the cerebellum in working memory and in spatial representation through hippocampal place cell activity suggests a possible role of the cerebellum in spatial working memory (SWM). We recently reported that Purkinje cells in the cerebellar LS and Crus I represent the phase and phase differences of neuronal oscillations in the medial prefrontal cortex (mPFC) and dorsal hippocampal dCA1 region (dCA1) [7], two structures known to be essential for SWM in rodents [8, 9]. The decision-making process during SWM tasks is associated with a brief increase in the coherence of neuronal oscillations in the mPFC and dCA1, and this coherence increase is believed to be essential for normal SWM decision making [10, 11]. Accuracy of SWM is essential for successfully navigating the environment and is therefore highly relevant for survival. We evaluated SWM performance and decision related mPFC-dCA coherence modulation in mice during spontaneous exploration of a plus-maze. SWM performance was quantified by counting spontaneous alternations, i.e. sequences of arm entries without repeating entry into a recently visited arm [12, 13].

We compared SWM performance and decision related mPFC-dCA1 coherence modulation in healthy control and mutant mice that have a selective loss of Purkinje cell neurotransmission [14] to determine

whether the cerebellum is required for SWM decision making and decision related mPFC-dCA1 coherence modulation. Moreover, optogenetic manipulation of LS Purkinje cell activity was used to determine whether Purkinje cell activity in cerebellar LS is causally involved in SWM decision making and decision-related mPFC-dCA1 coherence. Our findings suggest that the neuronal mechanism of cerebellar cognitive function involves a task specific cerebellar modulation of coherence of neuronal oscillations between cerebral cortical structures.

Methods

Animals

Thirty-two adult mice (18 males; 14 females) from 3 different strains were used in this study. One strain consisted of ataxic mice with genetically induced loss of Purkinje cell GABAergic neurotransmission ($L7^{Cre};Vgat^{flox/flox}$, n = 5) and their healthy littermate controls ($Vgat^{flox/flox}$, n = 5) [14]. A second strain selectively expressed Channelrhodopsin-2 (ChR2) in cerebellar Purkinje cells (Tg(Pcp2-COP4*H134R/EYFP)U126Isop/J) and was used for optophysiological activation of Purkinje cells in LS. We used two different light sources for optical stimulation of LS, an LED Chip (L7-ChR2$_{Chip}$, n = 8) and an LED-coupled optical fiber (L7-ChR2$_{Fiber}$, n = 9). Finally, C57BL/6J mice served as controls for optical stimulation with the LED Chip in the absence of ChR2 expression (C57BL/6J$_{Chip}$, n = 5). Table 1 summarizes the experimental groups, manipulations and analyses that were carried out.

One mouse in the L7-ChR2$_{Chip}$ group and one in the C57BL/6J$_{Chip}$ control group were included in the analysis of SWM behavior, but did not provide usable electrophysiological data (see asterisks in Table 1).

Mice were housed in a breeding colony at the University of Tennessee Health Science Center animal facilities with 12-hour light/dark cycles in standard cages with free access to food and water. All animal procedures were performed in accordance with the NIH Guide for the Care and Use of Laboratory Animals (2011). Experimental protocols were approved by the Institutional Animal Care and Use Committee.

Table 1. Experimental groups and treatments. *L7^{Cre};Vgat$^{flox/flox}$*: ataxic mutant, *Vgat$^{flox/flox}$*: non-ataxic littermate; L7-ChR2$_{Chip/Fiber}$: expressing channelrhodopsin2 in cerebellar Purkinje cells.

Group	n (M/F)	SWM test	Coherence analysis (no stimulation)	Coherence analysis w/opt. stim.	Light source	Opt. Stimulation frequency
L7^{Cre};Vgat$^{flox/flox}$	5 (5/0)	+	+			
Vgat$^{flox/flox}$	5 (1/4)	+	+			
L7-ChR2$_{Chip}$	8* (5/3)	+	+		Chip-LED	100 Hz
L7-ChR2$_{Fiber}$	9 (4/5)	+	+	+	Fiber-LED	120 Hz
C57BL/6J$_{Chip}$	5* (3/2)	+	+	+	Chip-LED	120 Hz

* One mouse each from the L7-ChR2$_{Chip}$ and C57BL/6J$_{Chip}$ groups were included in the analysis of behavior but excluded for coherence analysis due to unsuccessful electrophysiological recordings.

Surgery

Mice were surgically prepared for freely-moving electrophysiological recordings in the mPFC and dCA1 while performing a plus-maze SWM task. Surgical anesthesia was initiated by exposing mice to a mix of 3% isoflurane in oxygen in an induction chamber. Anesthesia was maintained with 1-2% isoflurane in oxygen during surgery using an Ohio isoflurane vaporizer (Highland Medical Equipment, Deerfield, IL,

USA). Body temperature was maintained at 37-38˚C with a servo-controlled heat blanket (FHC, Bowdoinham, ME, USA) monitored by rectal thermometer. At the beginning of each surgery, after mice were anesthetized but before the first incision, mice received a single subcutaneous injection of the analgesic Meloxicam SR (4 mg/kg, 0.06 ml) to alleviate pain. Two round skull openings (1.0 mm diameter) were prepared over the left mPFC (AP 2.46 mm; ML 0.5 mm) and the left hippocampus (AP -2.3 mm; ML 2.0 mm) using a dental drill (Microtorque II, RAM Products, Inc., USA), leaving the underlying dura intact. For mice in which optical stimulation was applied with a Chip-LED (L7-ChR2$_{Chip}$ and C57BL/6J$_{Chip}$) the bone overlying the right cerebellar LS (AP -6.0 mm; ML 2.0 mm) was thinned and the Chip-LED placed directly on the thinned bone. For mice stimulated with an optical fiber coupled LED (L7-ChR2$_{Fiber}$) a small opening was prepared overlying LS and the fiber was inserted to touch but not penetrate the dura. Two extracellular recording electrodes (glass insulated tungsten/platinum; 80 µm diameter; impedance: 3.5-5.0 MΩ) attached to a custom-made micro-drive were centered over the center of the mPFC and dCA1 skull opening and microdrives were fixed to the skull using dental cement. All four electrodes were connected to a 20-pin micro-connector (Omnetics Connector Corp.) Mice in the L7-ChR2$_{Chip}$, L7-ChR2$_{Fiber}$ and C57BL/6J$_{Chip}$ groups received additional implants of a chip-LED or an LED-coupled optical fiber (see section below for technical details) over the cerebellar LS. In addition, an acrylic head-post was mounted on the skull to provide a handle to manually stabilize the head while connecting and disconnecting the wireless headstage. The micro-drives, head-post and wire connectors were embedded in dental cement and anchored to the skull bone using three small skull screws. A postsurgical recovery period of 3-4 days was allowed before electrophysiological experiments began.

Behavioral task

The plus-maze task was used to quantify spatial working memory using counts of spontaneous alternations [12]. During spontaneous maze exploration healthy mice tend to avoid entering recently visited arms and generate arm-entry sequences without repetition at above-chance level. Such repeat-free

sequences called spontaneous alternations (Fig. 1). In a four-arm maze, like the plus-maze used here, random arm visits would result in 22.5% spontaneous alternations. Healthy mice or rats generate significantly higher numbers of spontaneous alternations and reduced percentage of spontaneous alternations is interpreted as a deficit in SWM [12, 13]. Mice explored the plus-maze for 12 min while the exploratory movements were automatically tracked using a video system (30 frames/s; Viewer, Biobserve GmbH). Arm entry sequences and resulting spontaneous alternations were analyzed off-line (Fig. 1).

Each mouse performed the plus-maze test 5 times, once per day on five successive days. The first session was for training purpose only and was not analyzed further. On the following days electrophysiological recordings were performed during each session. Mice in the three groups were prepared to also receive optical stimuli to cerebellar LS at the time of decision making (L7-ChR2$_{Chip}$, L7-ChR2$_{Fiber,}$ C57BL/6J$_{Chip}$). We alternated between days with and without optical stimulation. Whether optical stimulation was applied on days 1 and 3 or days 2 and 4 was pseudo-randomized. Each arm entry was classified as 'correct' or 'incorrect' based on whether it was part of a spontaneous alternation or represented a repeat entry (Figure 1).

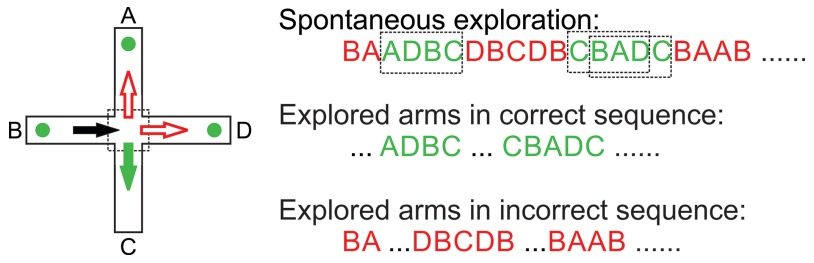

Figure 1. Schematic drawing of a plus-maze with arms labeled by letters and example arm-entry sequences shown on the right. Four consecutive arm-entries without repeats are considered a spontaneous alternation and are shown as green letter sequences framed by dashed rectangles in the examples. Arm-entries that are

part of a spontaneous alternation are considered correct choices. All other entries (red letters in the example sequences) are classified as incorrect choices. Arrows placed inside the plus maze drawing illustrate example choices: the mouse has explored three arms (A, B and D) and leaves arm B (black arrow). Entering C would be the correct choice (green arrow). Entering A or D would be an incorrect choice.

Electrophysiology

Electrophysiological recordings were conducted with extracellular recording electrodes (glass insulated tungsten/platinum; 80 µm diameter; impedance: 3.5-5.0 MΩ) attached to a custom-made micro-drive. Two electrodes each, separated by 0.25 mm, were placed in mPFC and dCA1. All four electrodes were connected to a 20-pin micro-connector (Omnetics Connector Corporation). During recording sessions, a wireless headstage (W2100-HS16, Multichannel Systems, Germany) was plugged into the miroconnector. To reduce the weight of the head mount, the battery was removed from the head stage. Power was supplied by connecting the battery and head stage with two highly flexible thin wires (2 m, 40 AWG solid nickel). Recordings were performed on five consecutive days. On the first day electrodes were manually advanced into the left mPFC and dCA1 while the animals were in their home-cage (Fig. 2a). After the final recording session recording sites were marked by small electrolytic lesions (10 µA DC; 12 s) and verified anatomically (Fig. 2b). Successful positioning of electrode tips in the dCA1 region was verified online by the presence of sharp wave ripples [15] (Fig. 2c). After electrodes were positioned, mice were placed in the plus-maze for 5 min to allow them to become familiar with the maze. On the following four days LFP activity in the mPFC and dCA1 was recorded while the animals explored the plus-maze. Prior to each recording session, while the mice were still in home-cage, LFP signals were evaluated and electrode positions were adjusted if necessary. Broad band voltage signals (0.1 – 8 kHz) were digitized at 20 kHz and saved to a hard-disk (W2100-HS16, Multichannel Systems, Germany). LFPs were bandpass filtered off-line at 0.1 – 200 Hz using Spike2 software (Cambridge Electronic Design Limited, UK).

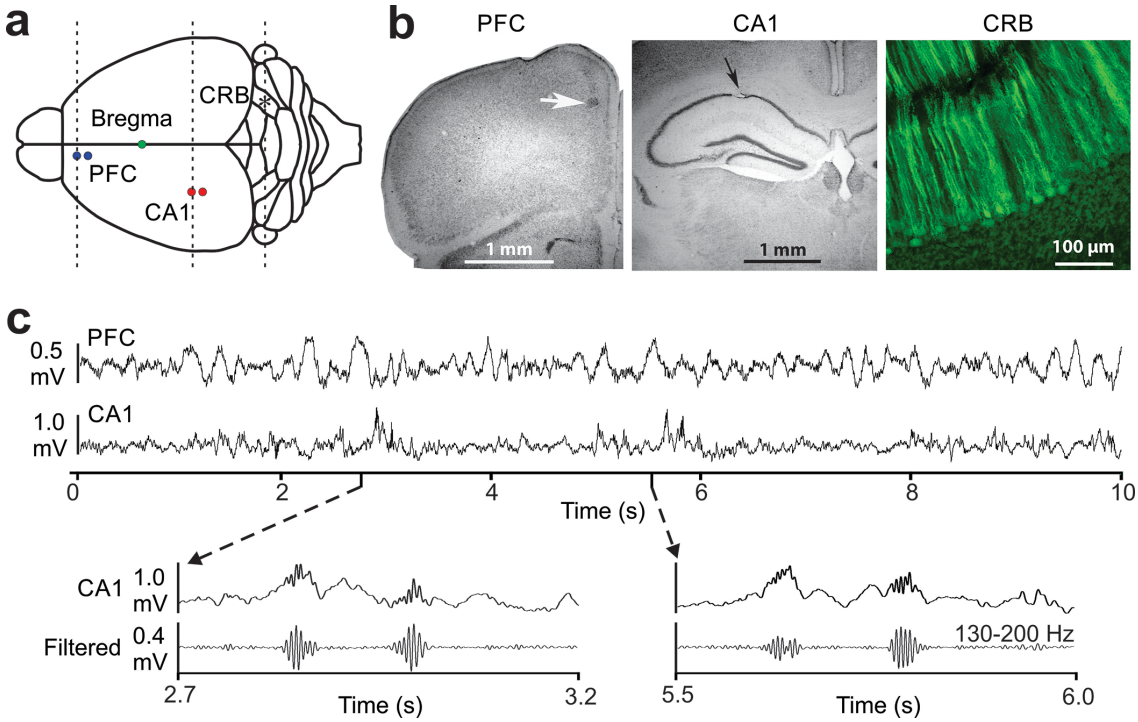

Figure 2. Illustration of recording locations and data examples. **(a)** Schematic drawing of the top view of a mouse brain. Local LFPs were recorded from the left mPFC and left dCA1 region of the hippocampus (dCA1). The star marks the site of optogenetic stimulation applied to the cortical surface of cerebellum (CRB). Dashed lines represent the coronal sections for verifying the recording locations in mPFC and dCA1 as well as the ChR2 expression in Purkinje cells. **(b)** Examples of electrolytic lesions (arrows) at recording sites in the mPFC and dCA1 region and L7-Chr2-GFP expression in Purkinje cells of the LS. **(c)** Examples of raw LFP signals recorded in mPFC and dCA1. Panels at the bottom show enlarged views of raw LFPs around ripple events in dCA1 (top traces) and band-pass filtered versions of the same LFP (130-200Hz) emphasizing the high-frequency component of sharp-wave ripple activity.

Optogenetic stimulation

During the plus-maze task with cerebellar stimulation, Purkinje cells in LS of L7-ChR2 expressing mice were photo-activated by applying a 1 sec light stimulus (sinusoidally modulated illumination, 100 Hz

or 120 Hz. Onset of the light stimulus was controlled by the experimenter and timed to occur with the mouse entering the center area of the plus maze. Two different LED devices, both emitting 465 nm light, were used for optical stimulation. A chip/micro SMD LED (1.25 x 2 mm, Lighthouse LEDs, LLC, WA, part # 10X12V0805PREWIREDBLUE) was used for optical stimulation in 8 L7-ChR2$_{Chip}$ mice and 5 C57BL/6J$_{Chip}$ mice. The Chip-LED was placed directly on the thinned bone overlying the LS and held in place with acrylic cement. An LED mounted on a 5 mm piece of optical fiber (200 micrometers diameter, Doric Lenses Inc., Quebec, Canada) was used for optical stimulation in 9 ChR2 expressing mice, with the optical fiber placed directly on the cortical surface of the LS without penetrating the dura. Optical stimulation with the two different light sources generated the same effects on behavior, but stimulation with the optical fiber assembly generated less electrical artifact in the electrophysiological recordings. Because of the electrical artifacts caused by chip-LED stimulation coherence during stimulation was only calculated for animals stimulated with the fiber coupled LED. The sinewave voltage used to control LED illumination was digitized (2 kHz) and recorded simultaneously with the electrophysiological data.

Data analysis

Raw data processing: Raw electrophysiological data were first processed for removing the powerline interference (60 Hz and harmonics) using a spectrum interpolation method [16, 17]. Data were then low pass filtered to create LFPs for further analysis (cutoff frequency: 200 Hz). All LFP signals were aligned at the time points (time 0s) that marked the mice were leaving the center area. For each task trial, 10s-LFP data (5s before and 5s after the 0s-datapoint) were selected and stored to a hard disk (at 2 kHz). The LFP data of L7-ChR2$_{Chip}$ group which received cerebellar stimulation of 100 Hz were excluded for analyzing the stimulation effect on LFP coherence because the stimulation artifact interferes with the high gamma band signals (80-90 Hz) reported in the present study.

Time-resolved coherence analysis of LFP: LFP signals from two recording sites, i.e. the mPFC and dCA1, were selected for time-resolved coherence analysis. All LFP data were first z-scored (Matlab function code: zscore). Time-resolved coherence was calculated in Matlab using custom scripts (Matlab R2019b; function code: *mscohere*; sliding window: 1 s; step size: 20 ms).

Time-frequency analysis of LFP: To examine time-frequency aspects of LFP activity in the mPFC and dCA1 region of the hippocampus, same z-scored LFP data that were used in coherence analysis were also analyzed using custom scripts (Matlab function code: *pspectrum*; Time resolution: 0.2 s).

Statistical analyses: All data were averaged for each mouse. Paired t-test and Two-Sample t-test were used to analyze changes in behavioral results of plus-maze task, coherence and power spectrum of LFP activities in the mPFC and dCA1. Figures represent results as mean ± standard error.

Histological evaluation of recording location

At the end of the experiments, animals were deeply anesthetized and intracardially perfused with 0.9% NaCl and followed by 4% paraformaldehyde solution. Brains were removed and fixed in 4% paraformaldehyde solution for a minimum of 24 hours. The accuracy of electrode penetrations was verified post-mortem for all animals by reference to surface maps of the location of cortical areas and hippocampus. For animals with marker lesions, the fixed brains were sectioned at 60 μm, mounted onto slides and Nissl stained. Light microscopy was used to verify the accurate depth of penetration of the recording electrode in the prefrontal cortex and the dCA1 region of the hippocampus (Fig. 2b).

Results

Reduced plus-maze task performance in mice with cerebellar deficit

We measured SWM performance in healthy mice and mice suffering from cerebellar ataxia induced by loss of Purkinje cell synaptic transmission. We first investigated whether the cerebellum is involved in the spatial working memory by comparing the plus-maze task performance of normal mice and those with cerebellar deficit. A total of twenty-two mice in the optogenetically manipulated groups (L7-ChR2$_{Chip}$, L7-ChR2$_{Fiber}$, C57BL/6J) were pooled as a normal behavior control group and compared with the cerebellar deficit mice (control and mutant groups). As shown in figure 3, during plus-maze tasks without cerebellar manipulation, the percentage of correct decision of C57BL/6J mice and of *Vgat*$^{flox/flox}$ mice were comparable (36.7% vs. 42.6%; p=0.112; two-sample test). In contrast, the percentage of correct decision in the *L7*^{Cre}*;Vgat*$^{flox/flox}$ mice with cerebellar deficit (mutant mice) was significantly reduced (21.2%).

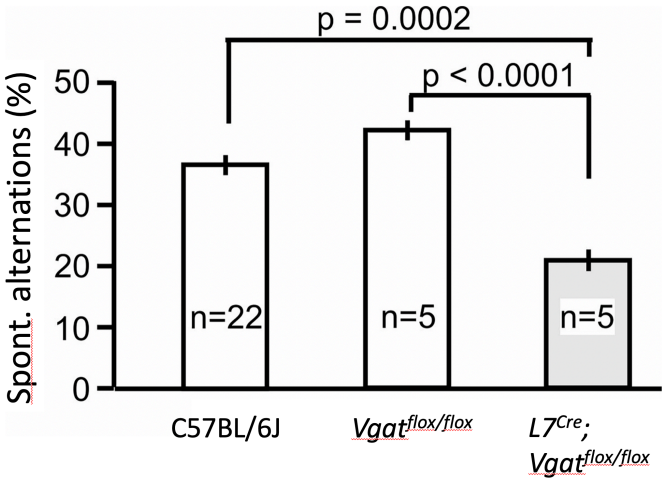

Figure 3. Plus-maze SWM task performance comparison between C57BL/6J mice, *Vgat*$^{flox/flox}$ control mice and ataxic *L7*^{Cre}*;Vgat*$^{flox/flox}$ mice. Bars represent mean percentage of spontaneous alternations in the sequence of arm entries. Error bars show ± standard error. P-values result from two-sample t-tests.

Abnormal coherence between mPFC and dCA1 during decision making in cerebellar deficit mice

Decision-related changes in coherence between the mPFC and dCA1 have been implicated in the process of SWM decision making and outcome. We analyzed time-resolved LFP coherence during SWM decision making, i.e. while animals were exploring the center area of plus-maze. We focused our analysis on data recorded during the two second period before the mice left center area of the maze. Leaving was defined as all four paws being inside the newly entered maze arm. Results show that, in $Vgat^{flox/flox}$ control animals at about about 0.8 s before leaving the center area, LFP coherences of gamma oscillations was linked to decision outcome. Coherence in the 80 – 90 Hz band increased to higher values for correct decisions compared to incorrect decisions (Figure 4, a,b,c). In the ataxic $L7^{Cre};Vgat^{flox/flox}$ mice, however, we did not observe a decision outcome related difference in gamma cochence (Figure 4, d,e,f). Thus, an intact cerebellum is required for both normal SWM performance and for SWM decision related mPFC-dCA1 coherence modulation.

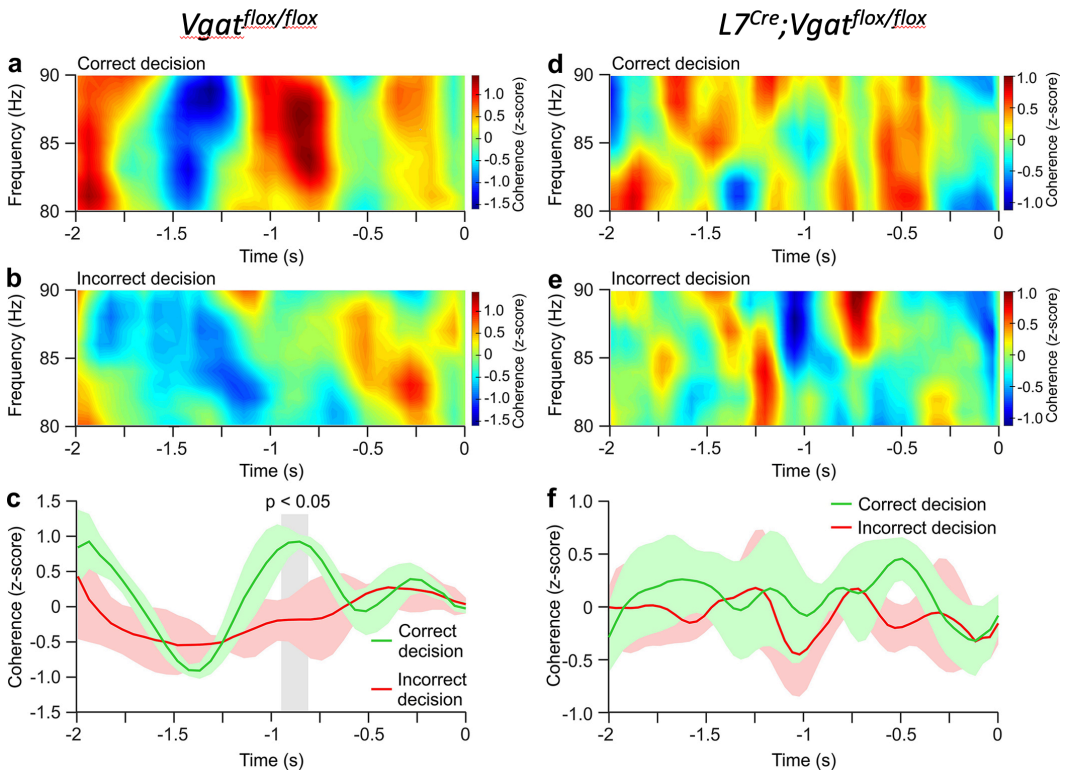

Figure 4. Time-resolved analysis of decision-related changes in coherence of gamma oscillations between mPFC and dCA1 during SWM decision making in a plus-maze. **a,** Pseudo-color plot showing coherence of mPFC-dCA1 oscillations between 80 and 90 Hz during correct SWM decisions in healthy *Vgat*$^{flox/flox}$ control mice. Time zero on the x-axis corresponds to the moment the mouse is leaving the center. **b**. As in **a** but for incorrect decisions. **c**. Coherence in **a** and **b** averaged across frequencies (80-90Hz). Green and red graphs show the mean coherence time courses for correct and incorrect decisions, respectively. Shaded areas represent ± standard error. **d, e**, **f**. As for **a-c** but for ataxic *L7*^{Cre}*;Vgat*$^{flox/flox}$ mice. Vertical gray bar in **c** indicates a time period with significant differences in coherence between correct and incorrect decision (Paired t-tests).

Changes in plus-maze task performance in mice following optogenetic activation of cerebellar lobulus simplex (LS)

To determine whether the cerebellum and specifically the cerebellar LS is causally involved in the modulation of mPFC-dCA1 gamma coherence we employed optogenetic stimulation of Purkinje cells in the LS during the process of SWM decision making. We used two types of light sources, a Chip-LED placed directly on the thinned bone overlying LS and a fiber coupled LED with the tip of the fiber touching the dura overlying the LS. Photoactivation of LS Purkinje cells was controlled manually by the experimenter and occurred at the moment the mouse's nose entered the center of the plus maze and lasted for one second (see methods). Stimulation of LS Purkinje with the two different light sources had similar effects on SWM performance, causing a decrease of SWM performance to chance levels (Fig. 5). When comparing trials with and without stimulation, the percentage of spontaneous alternations dropped from 34.6% to 20.6% for mice stimulated with the Chip-LED (L7-ChR2$_{Chip}$, Fig. 5 a) and from 38.3% to 24.3% for mice stimulated with the fiber coupled LED (L7-ChR2$_{Fiber}$, Fig. 5 b). When optical stimulation with a Chip-LED was applied to C57BL/6J mice that did not express channelrhodopsin (C57BL/6J$_{Chip}$) we found no difference in SWM performance between stimulated and non-stimulated trials (36.9% vs. 39.0%; Fig. 5 c).

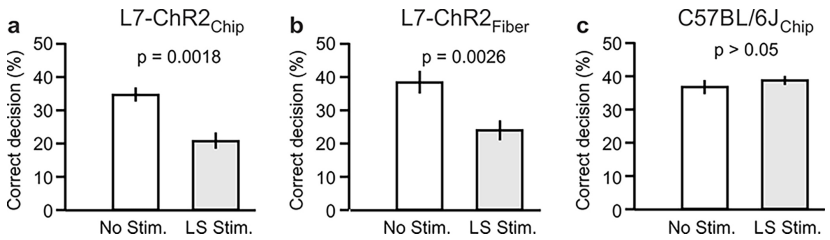

Figure 5. Effects of optogenetic cerebellar activation on plus-maze task performance in mice. **a.** Cerebellar stimulation (CRB-ST) with Chip-LED (L7-ChR2$_{Chip}$; n = 8); **b.** CRB-ST with optical fiber (L7-ChR2$_{Fiber}$; n = 9); **c**. CRB-ST with Chip-LED in control mice (C57BL/6J$_{Chip}$; n = 5); Data are expressed as mean ± standard error. P-values represent paired t-tests.

Optogenetic stimulation of cerebellar LS modulates mPFC-dCA1 coherence during decision-making

During the process of SWM decision making gamma coherence between the mPFC and dCA1 showed characteristic modulations that differed between correct and incorrect decisions in that incorrect decisions were associated with lower coherence values (Fig. 6 a-c). The differences in coherence values were significant during the period of about 0.7-1.3 s before the mice left the center area (Fig. 6 c). A power spectrum analysis of the LFP signals showed an increase in gamma power (80-90Hz) in the mPFC during correct decisions but not during incorrect decision (Fig. 6 g). No such decision outcome related difference in gamma power was observed in the dCA1 LFP (Fig. 6 h). When LS Purkinje cells were photoactivated during decision making, decision related differences in coherence modulation were no longer observed (Fig. 6 d,e,f), demonstrating a causal involvement of LS Purkinje cells in the modulation of decision related mPFC-dCA1 coherence and SWM performance. The increase in gamma power in the mPFC associated with correct decisions was also eliminated by photoactivation of LS Purkinje cells, while the stimulus did not change gamma power modulation in dCA1 (data not shown).

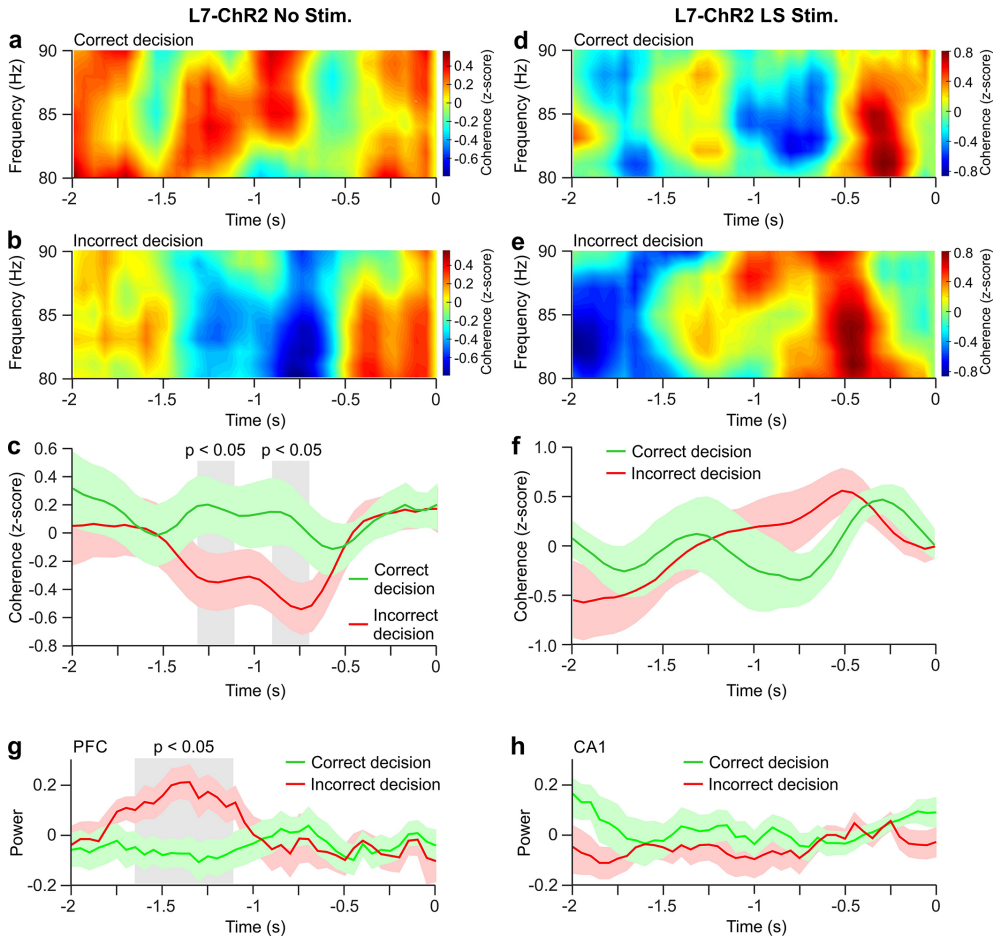

Figure 6. Time-resolved analysis of decision-related changes in mPFC-dCA1 gamma coherence during the plus-maze SWM task performance with and without optical stimulation of LS Purkinje cells in healthy mice. All results shown are from mice expressing channelrhodopsin2 in Purkinje cells which were implanted with a fiber-coupled LED (L7-ChR2$_{Fiber}$) for optical stimulation. **a, b.** Pseudo-color plots showing coherence of mPFC-dCA1 gamma oscillations (80 - 90 Hz) during choices of a correct (**a**) or incorrect (**b**) arm of the plus maze. Time zero corresponds to the time the mouse is leaving the center area, i.e. all four paws have left the center and entered the next arm. **c**. Coherence values in **a** and **b** averaged across frequency, showing the time course of mean gamma coherence during correct (green) and incorrect (red) decisions. Gray shaded areas mark epochs of significant differences between the two coherence functions. **d, e**, **f**.: As in **a, b** and **c.** Decision related coherence modulation of mPFC-dCA1 gamma oscillations when LS Purkinje cells were optically stimulated during the SWM decision making process. **g,**

h. Mean power of gamma oscillations (80-90 Hz) of LFPs in the mPFC (**g**) and dCA1 (**h**) during SWM decision making without optical stimulation. Gray shaded area in **g** marks epoch of significant differences between the two functions. Data in **c**, **f, g** and **h** are expressed as mean ± standard error. P-values represent paired t-tests. Shaded areas indicate epochs of significant differences.

Discussion

The cerebellum has been implicated in a broad spectrum of cognitive functions and extensive connections between the cerebellum and association cerebral cortical areas provide the anatomical basis for cerebrocerebellar interactions during cognitive processes [18, 19]. However, the neuronal mechanism of cerebrocerebellar communication during cognitive tasks has yet to be identified.

Here we presented causal evidence that the cerebellar LS is involved in the decision-making process during a spatial working memory (SWM) task in mice. SWM is a survival-critical cognitive function that requires both the mPFC and dCA1 in rodents [20-23].

We show that coherence of gamma oscillations in the mPFC and dCA1 increases during SWM decision making in healthy mice when they choose which arm to enter next in a plus maze spontaneous alternation task. Decision-related coherence increased to higher values when the mouse made a correct decision compared to entering an incorrect, i.e. recently visited maze arm. Hence, the magnitude of decision related coherence modulation was reflected decision outcome. Ataxic mice lacking Purkinje cell synaptic transmission [14] performed at chance level in the plus maze SWM task and decision related changes in coherence were no longer correlated with decision outcome. We provided causal evidence of an involvement of cerebellar LS in SWM decision making and in the modulation of mPFC-dCA1 coherence modulation by stimulating LS Purkinje cells during SWM decision making. This manipulation resulted in chance level SWM performance and the loss of decision-outcome related differences in mPFC-dCA1 coherence modulation. Our findings thus suggest that the cerebellum is involved in coordinating the

coherence of gamma oscillations between the mPFC and dCA1 at the time a mouse has to make a decision about which maze arm to enter, based on spatial working memory of the previous entries. In a previous study we have shown that simple spike activity of Purkinje cells in LS and in Crus I of the right cerebellum in mice represent the instantaneous phases and phase differences of oscillations in the mPFC and dCA1[7]. Based on those findings we suggest a role of the cerebellum in modulating coherence of oscillations between cerebral cortical structures. Popa et al. have previously shown that the cerebellum is required for normal gamma coherence between sensory and motor cortical areas in the mouse [24]. Our current findings support a role of the cerebellum as a coordinator of cerebral cortical functional connectivity by modulating the coherence of oscillations [25]. It is important to note that such a role of the cerebellum is very much in line with traditional views of cerebellar function, as the coordination of phase-relationships between two oscillations is a temporal coordination task. Cerebellar coordination of cerebral-cortical coherence thus may represent a general principle of cerebro-cerebellar neuronal interaction, that could in theory apply to both cognitive and sensorimotor tasks.

References:

1. Ashida, R., Cerminara, N.L., Edwards, R.J., Apps, R. & Brooks, J.C.W. Sensorimotor, language, and working memory representation within the human cerebellum. *Hum Brain Mapp* (2019).

2. Yu, W. & Krook-Magnuson, E. Cognitive Collaborations: Bidirectional Functional Connectivity Between the Cerebellum and the Hippocampus. *Front Syst Neurosci* **9**, 177 (2015).

3. Tomlinson, S.P., Davis, N.J., Morgan, H.M. & Bracewell, R.M. Cerebellar contributions to spatial memory. *Neurosci Lett* **578**, 182-186 (2014).

4. Rochefort, C*., et al.* Cerebellum shapes hippocampal spatial code. *Science* **334**, 385-389 (2011).

5. Watson, T.C.*, et al.* Anatomical and physiological foundations of cerebello-hippocampal interaction. *eLife* **8** (2019).

6. Lefort, J.M.*, et al.* Impaired cerebellar Purkinje cell potentiation generates unstable spatial map orientation and inaccurate navigation. *Nat Commun* **10**, 2251 (2019).

7. McAfee, S., Liu, Y., Sillitoe, R.V. & Heck, D.H. Cerebellar lobulus simplex and Crus I differentially represent phase and phase difference of prefrontal cortical and hippocampal oscillations. *Cell reports* **27**, 2328–2334 (2019).

8. Lee, I. & Kesner, R.P. Time-dependent relationship between the dorsal hippocampus and the prefrontal cortex in spatial memory. *J Neurosci* **23**, 1517-1523 (2003).

9. Churchwell, J.C. & Kesner, R.P. Hippocampal-prefrontal dynamics in spatial working memory: interactions and independent parallel processing. *Behav Brain Res* **225**, 389-395 (2011).

10. Gordon, J.A. Oscillations and hippocampal-prefrontal synchrony. *Curr Opin Neurobiol* **21**, 486-491 (2011).

11. Spellman, T.*, et al.* Hippocampal-prefrontal input supports spatial encoding in working memory. *Nature* **522**, 309-314 (2015).

12. Richman, C.L., Dember, W.N. & Kim, P. Spontaneous Alternation Behavior in Animals: A Review *Current Psychological Research & Reviews* **5**, 358-391 (1987).

13. Lalonde, R. The neurobiological basis of spontaneous alternation. *Neurosci Biobehav Rev* **26**, 91-104 (2002).

14. White, J.J.*, et al.* Cerebellar zonal patterning relies on purkinje cell neurotransmission. *J Neurosci* **34**, 8231-8245 (2014).

15. Buzsaki, G. Hippocampal sharp wave-ripple: A cognitive biomarker for episodic memory and planning. *Hippocampus* **25**, 1073-1188 (2015).

16. Mewett, D.T., Reynolds, K.J. & Nazeran, H. Reducing power line interference in digitised electromyogram recordings by spectrum interpolation. *Medical & biological engineering & computing* **42**, 524-531 (2004).

17. Leske, S. & Dalal, S.S. Reducing power line noise in EEG and MEG data via spectrum interpolation. *Neuroimage* **189**, 763-776 (2019).

18. Schmahmann, J.D. The cerebellum and cognition. *Neurosci Lett* **688**, 62-75 (2019).

19. Buckner, R.L. The cerebellum and cognitive function: 25 years of insight from anatomy and neuroimaging. *Neuron* **80**, 807-815 (2013).

20. Negron-Oyarzo, I.*, et al.* Coordinated prefrontal-hippocampal activity and navigation strategy-related prefrontal firing during spatial memory formation. *Proc Natl Acad Sci U S A* **115**, 7123-7128 (2018).

21. Wirt, R.A. & Hyman, J.M. Integrating Spatial Working Memory and Remote Memory: Interactions between the Medial Prefrontal Cortex and Hippocampus. *Brain Sci* **7** (2017).

22. Benchenane, K., Tiesinga, P.H. & Battaglia, F.P. Oscillations in the prefrontal cortex: a gateway to memory and attention. *Curr Opin Neurobiol* **21**, 475-485 (2011).

23. Jones, M.W. & Wilson, M.A. Theta rhythms coordinate hippocampal-prefrontal interactions in a spatial memory task. *PLoS Biol* **3**, e402 (2005).

24. Popa, D.*, et al.* Functional role of the cerebellum in gamma-band synchronization of the sensory and motor cortices. *J Neurosci* **33**, 6552-6556 (2013).

25. Fries, P. Rhythms for Cognition: Communication through Coherence. *Neuron* **88**, 220-135 (2015).

Acknowledgements

D.H.H. and Y.L. are supported by R01MH112143, R01MH112143-02S1 and R37MH085726. R.V.S. is supported by R01NS089664, R01NS100874, R01MH112143 and U54HD083092. [##Stu, enter any funding

source here##]. We would like to thank the Neuroscience Institute of the University of Tennessee Health Science Center (UTHSC) for financial support and Micheal Nguyen from the UTHSC Bio-Medical Services for technical support.